

Chapter 2

Methods

2.1 Equilibrium Measurements

To examine protein binding to DNA, first the steady-state fluorescence emission spectra were measured using a FluoroMax-4 spectrofluorimeter (81005, Horiba Scientific) on fluorescence-labeled DNA samples in the presence and absence of protein. The spectral differences between free DNA and protein–DNA complex can be correlated both with the extent of protein binding and with the protein-induced conformational changes in DNA at equilibrium. To examine the thermal dissociation of the complex, and to determine the temperatures at which to carry out laser T-jump studies, equilibrium measurements were done as a function of temperature for all protein–DNA complexes studied in this thesis.

2.2 Laser Temperature Jump Technique

Laser-induced temperature jump relaxation spectroscopy has emerged as a very useful technique to probe the conformational dynamics of biomolecules (protein, DNA, RNA) and the dynamics of the interactions between them. The basic idea behind this approach is that the equilibrium of interconverting chemical species is suddenly perturbed with a temperature jump, forcing the system to establish a new equilibrium point at a higher temperature. The change in the populations of the interconverting species as they evolve in response to the T-jump perturbation can be monitored with a suitable spectroscopic probe attached to the biomolecule. This time-resolved spectroscopy enables us to follow the conformational dynamics of the biomolecules over an enormous time-window from few nanoseconds to several milliseconds. This T-jump perturbation must be fast in comparison with the conformational dynamics of interest. Dynamical interactions relevant to the function of a biomolecule can take place on time scales from sub-microseconds to several

seconds or longer. Using a pulsed laser excitation with pulses in the near-IR range, where water absorbs, it is possible to induce a fast T- jump perturbation in aqueous samples. Since vibrational relaxation takes place on the picosecond time scale both in water and in biomolecules, complete thermalization of solvent and solute occurs in 10–20 ps time scale [1]. However, since we use a laser pulse of 10 ns, the temperature of the sample volume reaches its maximum value within 10–20 ns. In this case, the dead time of the T-jump apparatus is determined by the IR laser pulse width convoluted with the response time of the detection electronics.

In 1964, Eigen and Demayer designed the first T-jump technique based on the electrical discharge of a capacitor through a conducting solution. The heating time in this setup is determined by the RC (R-resistance, C- capacitance) of the capacitor circuit and is typically on the order of microseconds for a temperature jump of a few degrees. The discovery of pulsed lasers in the 1960s led to an alternative way of directly heating the solution by an intense light pulse. Since the emission wavelengths of then available ruby (694 nm) and Nd:glass (1060 nm) lasers are not absorbed by water, the earlier studies were done in the presence of strongly absorbing dyes in the sample solution to produce heating [2–4]. Adding the dyes in samples may pose some problems as the dyes may interfere with the reaction process of the samples, and it can also interfere with the spectroscopic probing of the reaction by overlapping the spectral signals. Therefore, the desirable method is directly heating the solvent. Direct heating of the aqueous solvent required near-infrared pulses with several mJ of energy between 1300 and 2100 nm to excite the overtone of the OH stretching band [5].

The laser we have been using in our T-jump setup is an Nd:Yag laser with a fundamental wavelength of 1064 nm. Laser pulses at the desirable wavelength are obtained by Raman conversion (Fig. 2.1). Raman scattering is the elastic light scattering where the energy (and hence the frequency) of the scattered photon is shifted with respect to that of incident photon by the vibrational (or rotational) frequency of the gas medium [5]. The frequency shift occurs when some of the energy of the scattered photon is taken up by a molecule, which is excited into vibrational motion. The frequency can decrease (giving rise to Stokes lines) or increase (anti-Stokes lines) by integer multiples of the vibrational frequency of the medium, depending on whether the molecule start in the ground state or an excited state. Initially, most of the molecules would be in the ground state, with some molecules in the excited states due to thermal fluctuations. Since the initial population of the excited states is usually very small, the anti-Stokes lines are much weaker than the Stokes lines. When the incident laser beam power is sufficiently high, the intensity of the Stokes radiation reaches the threshold. At this point, the Raman Effect becomes stimulated. The stimulated Stokes beam behaves like a laser emission (coherent and propagates in the direction of the pump beam). This is a relatively simple and useful method to extend the wavelength range of the existing laser source. In our apparatus, we use a 1 m long Raman cell containing high pressure (400 psi) methane gas, which shifts the Nd:Yag fundamental (1064 nm) to 1542 nm, 2800 nm, etc. and anti-Stoke lines to 812, 656 and 474 nm. The first Stoke's line at 1542 nm is the desired wavelength to heat the aqueous samples and

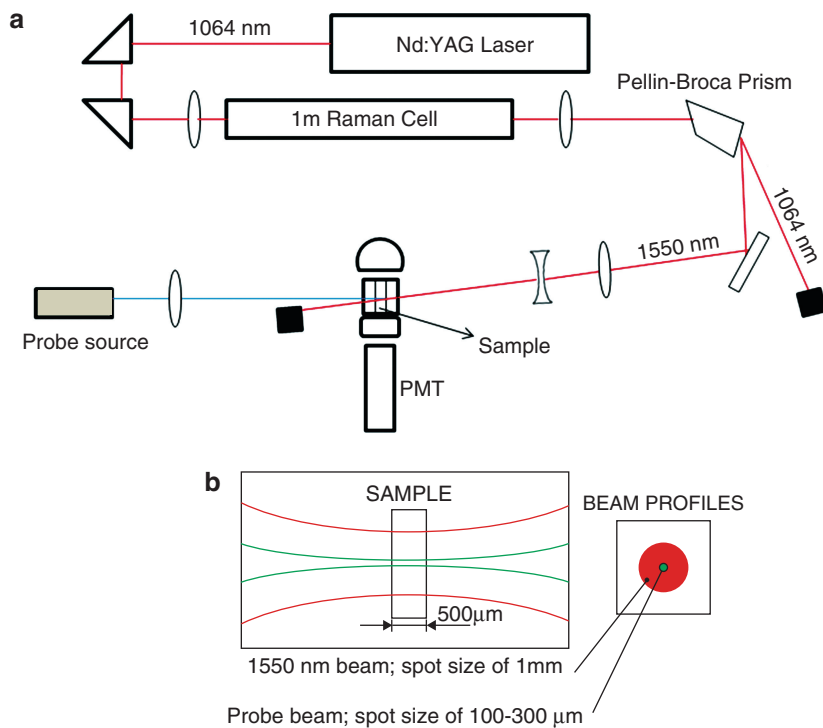


Fig. 2.1 (a) Schematic of laser temperature jump spectrometer setup. (b) IR beam profile (*red*) (spot size 1 mm) and probe beam profile (*green*) (spot size 100–300 μm) at the sample position. Three different probe beam sources were used in this thesis (1) Xe-Hg lamp, (2) 488 nm diode laser, (3) 532 nm diode laser

is separated from the other lines that emerge from the Raman cell by a Pellin–Broca prism. The conversion efficiency of the Raman cell is 15 %. Hence in our T-jump setup, we get energy of ~50 mJ/pulse at the sample position if we start with ~300 mJ/pulse laser energy at 1064 nm, incident on the Raman cell.

2.2.1 Laser Temperature Jump Spectrometer

For all kinetic measurements on fluorescein dye-labeled DNA, the probe source to monitor the fluorescence intensity was a 20 mW CW diode laser at 488 nm (Newport PC13589) or a 50 mW 532 nm diode laser (Crystal Laser LC, GCL-050-L). The diode laser beam was focused directly on to the sample, to a spot size of 100 μm, and aligned to fall at the center of the 1 mm diameter heated

spot produced by the IR beam. For kinetic measurements that probed fluorescent nucleotide analogues incorporated in DNA (e.g., 2AP or tC^o probes, as described in Sects 2.3 and 2.4), the probe source was a 200 W-Xe/Hg lamp. The light from the Xe/Hg lamp was first focused on to a 300 μm aperture, and the aperture was then reimaged on to the sample at the center of the 1 mm diameter heated spot. In the case of lasers, we were able to directly focus the beam at sample position with the focal-spot diameter of ~ 100 μm as the beam profile from the laser was a well-defined collimated beam with the diameter of ~ 1 cm after it passes through a beam expansion lens. However, in the case of the UV lamp, we needed an aperture, as the beam output from the lamp was much wider (~ 2 cm) and hence, we used a 300 μm aperture to reimage it at the sample position. The sample cuvettes of rectangular cross-sections of 0.5 mm by 2 mm and height 20 cm were designed from quartz glass tubes, which were then cut to smaller pieces (lengths of 3 cm) and sealed at one end (at the UIC Chemistry Department glass shop). The samples were oriented such that the path length through which the IR beam and the probe beam traversed was 0.5 mm, while the surface facing the IR beam (on one side) and the probe beam (on the other side) had dimensions 2 mm across and 3 cm high. The typical volume of the sample required in these cuvettes was ~ 40 μL . The equilibrium temperature of the sample was controlled by a heat bath (TRE 111 from Neslab). The transient temperature of the sample after the heater pulse was measured as described in Sect. 2.2.4.

The fluorescence emission is collected 90° to the excitation direction and focused on a photomultiplier (Hamamatsu 12928) after passing through band pass filters designed to transmit around the fluorescence emission maximum, while rejecting any stray fundamental or Stokes/anti-Stokes lines. However, complete elimination of the stray light has been one of the challenges we face in our spectrometer, and during kinetics measurement this stray light saturates the PMT tube and basically limits the time-resolution of the T-jump apparatus to 10–20 μs , even though in principle we should be able to get the time-resolution of 200 ns with the slow amplifier and 10 ns with the fast amplifier. The photomultiplier tube is coupled to either a 5 MHz preamplifier (C1053-51, Hamamatsu) when the probe source was the Xe/Hg lamp, or a 300 MHz preamplifier (SR445A, Stanford Research) when the probe source was the diode laser. The signal from the PMT was digitized using a 500 MHz transient digitizer (Hewlett Packard 54825A), which was recently replaced by a new digitizer from Tektronix (DPO 4054B). For each kinetic trace at a given initial temperature, typically over 500 shots (each with 20,000 data points from the HP digitizer or one million data points from the Tektronix digitizer) were averaged together. In order to minimize photo damage to the dye molecules, a fast mechanical shutter (UniBLITZ, VS14) was employed to block the probe beam between acquisitions of laser pulses. For each laser shot, the shutter was kept open for ~ 60 –450 ms depending on the kinetics time scale of a particular interaction. The averaged kinetics traces from the digitizer were transferred to a computer for further analysis.

2.2.2 Theoretical Estimation of the Size of the T-Jump

The temperature increase upon the absorption of energy from the infrared laser pulse by the sample is given by

$$\Delta T = \frac{I_a}{\rho V C_w} \quad (2.1)$$

In Eq. (2.1), I_a is the absorbed intensity by the sample, ρ is the density of the absorbing medium, C_w is the specific heat, and V is the volume of sample which absorbed the energy. In writing this equation, we have assumed that the incident energy is absorbed uniformly throughout the volume.

If an incident radiation I_o passes through a substance of thickness l and molar concentration C , then the transmitted intensity is given by the Beer–Lambert law

$$I_t = I_o 10^{-OD} \quad (2.2)$$

where $OD = \epsilon l C = \alpha l$ and $\alpha = \epsilon C$

The absorbed intensity I_a is thus given by

$$I_a = I_o - I_t \quad (2.3)$$

$$I_a = I_o (1 - 10^{-\alpha l}) \quad (2.4)$$

which yields

$$\Delta T = \frac{I_o (1 - 10^{-\alpha l})}{\rho V C_w} \quad (2.5)$$

In our experimental setup, $I_o \approx 50$ mJ at 1554 nm, and this energy is absorbed by the aqueous solution of $\alpha \approx 0.52 \text{ mm}^{-1}$ [6], $\rho = 1 \text{ g/cm}^3$, and $C_w = 4.186 \text{ J/(g } ^\circ\text{C)}$. If we assumed that the heated volume is a cylinder with radius ~ 0.5 mm, ignoring the Gaussian beam profile of the focused IR spot and use the path length of the sample $l = 0.5$ mm, we obtain $\Delta T \approx 12$ $^\circ\text{C}$. This T-jump agrees reasonably well with the T-jump of ~ 5 – 10 $^\circ\text{C}$ that we obtain during our experiments, measured using a reference sample, as described in Sect. 2.2.4. The primary reasons for the lower than expected T-jump under our experimental conditions are most probably due to imperfect alignment between the IR beam and the probe beam, fluctuations in beam alignment due to lamp (probe source) drifting or unstable IR beam over time.

In principle, we can increase the size of the T-jump by increasing the incident laser beam energy or by focusing the beam more sharply on the sample. However, large T-jumps (> 20 $^\circ\text{C}$) also create undesirable effects such as photo-acoustic effects and cavitation, as discussed below.

2.2.3 Photo-Acoustic Effects and Cavitation

A rapid temperature jump can produce large pressure within the heated volume. This pressure can reach well over 100 bar [7]. The shock wave (photo-acoustic) produced by the rapid increase in the pressure propagates outwards and reflects back from the walls of the sample cell and produce large oscillations of the density of refractive index in the probed volume. In aqueous solution, the time scale of these events is given by the speed of the sound and the cell geometry [5]. The photo-acoustic effect in the observed signal intensity can be seen as damped periodic oscillations. If these oscillations were present in the kinetic traces during the T-jump experiment, then the focusing of the infrared beam with respect to probe beam was realigned until the oscillations disappeared from the trace.

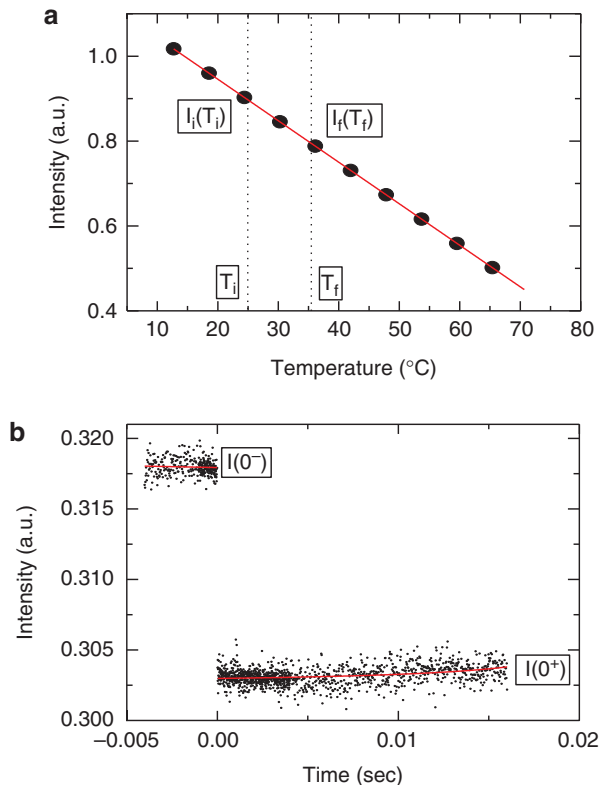
Another problem caused by large T-jumps is cavitation. When the short laser pulse produces local heating, the pressurized liquid expands outward, the pressure within the heated volume drops to negative (tensile) values. When the tensile pressure reaches 5–10 bar, it exceeds the cavitation threshold, which in turn results in nucleation and growth of bubbles in the fluid medium [5]. The initial negative pressure peaks around 100 ns after the pulse and cavitation effects are usually observed for several microseconds. Bubbles with maximum diameters up to 100 μm can be generated [5]. These bubbles can defocus the incident probe beam or deflect it away from the PMT, resulting in a dramatic decrease in the detected signal, which appears as an additional transient in the measured kinetic trace. Cavitation effects can be reduced by filtering the sample and thoroughly degassing it, which helps to eliminate possible nucleation sites.

Both photo-acoustic oscillations and cavitation effects, if they persist, typically last for about 20–30 μs , thus hampering the time-resolution of our measurements.

2.2.4 Estimation of Temperature Jump Using Reference Sample in a T-Jump Experiment

The magnitude of the T-jump in our apparatus, for a given alignment, is estimated using a reference sample (e.g., donor-only-labeled single-stranded (ss) or duplex DNA or free fluorescence dye). Ideally, free dye samples are preferable since they exhibit only a temperature-dependent change in quantum yield as the temperature of the sample is raised, which can be used to estimate the size of the T-jump as described below. In contrast, ssDNA may form hairpin structures that can unfold as a result of the T-jump perturbation, thus exhibiting unwanted relaxation kinetics in the control experiments. Similarly, duplex DNA may exhibit DNA melting/pre-melting kinetics at high enough temperatures. In Chap. 4, we used probes incorporated double-stranded DNA samples as a control since this particular dye in free form was not commercially available. However, the DNA melting temperatures for these DNA constructs are much higher ($>70^\circ\text{C}$) compared to our T-jump temperature window, and therefore these samples behave well during the T-jump measurements.

Fig. 2.2 (a) Fluorescence intensity as a function of temperature of a free fluorescein dye sample under equilibrium conditions. (b) Intensity as a function of time as a result of a $\sim 5^\circ\text{C}$ T-jump



As illustrated in Fig. 2.2a, first the donor fluorescence intensity of the control sample as a function of temperature is obtained under equilibrium conditions, as described in Sect. 2.1. The fluorescence intensity typically decreases linearly with increasing temperature. As an example, for free fluorescein, the fluorescence decreases by $\sim 1\%$ for every degree increase in temperature (Fig. 2.2a). T-jump experiment on free fluorescein (Fig. 2.2b) shows the fluorescence intensity level $I(0^-)$ measured at the initial (equilibrium) temperature of the sample before the arrival of the heater pulse (the pre-laser level), followed by a rapid drop in the fluorescence intensity immediately after the arrival of the heater pulse to a post-pulse level $I(0^+)$, as a result of the rapid increase in the temperature of the sample. The fluorescence intensity then stays approximately the same up to about 20 ms, after which it slowly recovers to the pre-heater-pulse level with a time constant of ~ 200 ms (Fig. 2.4), concurrent with the recovery of the sample temperature back to its pre-T-jump equilibrium value.

To estimate the size of the T-jump, we compare the fluorescence intensities at the initial (T_i) and final (T_f) temperatures, denoted by $I_i(T_i)$ and $I_f(T_f)$ in equilibrium experiment, Fig. 2.2a, with the intensities before and after the T-jump, $I(0^-)$

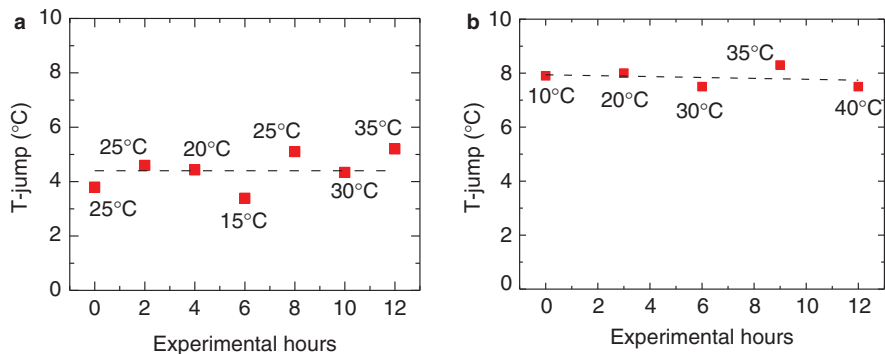


Fig. 2.3 (a) The magnitude of the T-jump measured on a control sample consisting of a short 3-nt long DNA oligomer containing 2-aminopurine (TXA with 2AP at the position labeled X). The measurements were done every 2 h over a period of 12 h. The initial equilibrium temperature before the T-jump was varied between 15 and 35 °C as shown in the figure (heating pulse is from an old IR laser). (b) The same experiment as in (a) was repeated with a new IR laser, which shows very stable IR beam energy and hence reflects as a stable high temperature jump (measured with a free 2AP reference sample)

and $I(0^+)$, respectively, in the T-jump experiment. The relationship between the intensities from the equilibrium and T-jump measurements, given by:

$$\frac{I_f(T_f)}{I_i(T_i)} = \frac{I(0^+)}{I(0^-)} \quad (2.6)$$

is used to estimate the value of $I_f(T_f)$ in terms of the experimentally measured $I_i(T_i)$, $I(0^-)$, and $I(0^+)$, and interpolated on the equilibrium fluorescence intensity versus temperature plot of Fig. 2.2a to obtain the final temperature T_f . Figure 2.3 shows the fluctuations in T-jump values measured on a 2AP-labeled control sample during a 12 h experimental period using an old IR laser (A) and new IR laser (B) and demonstrates the stability of the alignment in the T-jump apparatus over the course of a typical experiment.

2.2.5 T-Jump Recovery Kinetics

Measurements on control samples taken over a longer time-window (up to about 800 ms) show the “T-jump recovery kinetics,” which is the relaxation of the temperature of the heated volume of the sample back to its pre-laser equilibrium level. A representative recovery trace (shown in Fig. 2.4) reveals that the temperature stays high up to about 10–20 ms before it starts to recover.

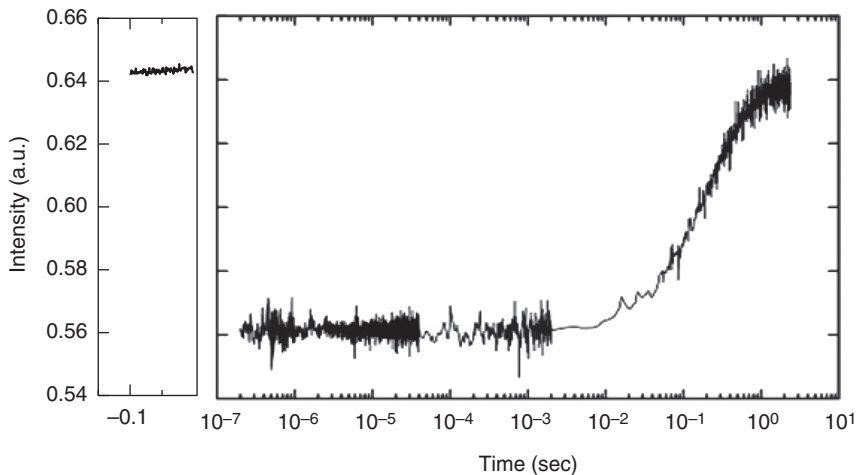


Fig. 2.4 Kinetics trace from a control experiment (free fluorescent dye sample) plotted on logarithmic time scale to illustrate the recovery of the temperature to the initial T_i

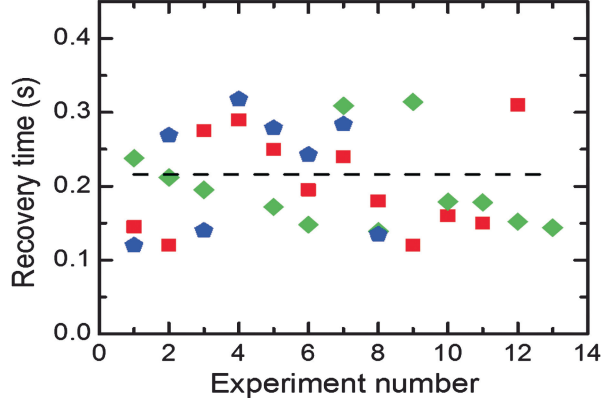
The recovery kinetics is well described by the following recovery function:

$$I(t) = [I(0^+) - I(0^-)]f_{\text{rec}}(t) + I(0^-) \quad (2.7)$$

with $f_{\text{rec}}(t) = (1 + t/\tau_{\text{rec}})^{-1}$, where τ_{rec} is a characteristic time for the decay of the T-jump. This functional form of the recovery function is an empirical function that was found to fit the T-jump recovery kinetics slightly better than a single-exponential decay function. $I(0^+)$ and τ_{rec} were varied as free parameters in a nonlinear least-squares fit to the T-jump recovery traces obtained on control samples. The recovery time constant τ_{rec} was determined for each sample from the average of several such measurements. Figure 2.5 shows a range of recovery times obtained from measurements on several different reference samples, over the course of 72 months. The average value of the recovery time constant from these set of measurements is found to be $\tau_{\text{rec}} = 215 \pm 105$ ms.

In general, kinetic processes that occur with relaxation times smaller than ~ 20 ms are not significantly disturbed by the T-jump recovery response of the apparatus. However, if the amplitude change in fluorescence from the relaxation kinetics of interest is significantly smaller than the change in fluorescence from the T-jump itself (which is proportional to the temperature-dependent quantum-yield change of a particular dye), then the T-jump recovery kinetics can have an appreciable interference with the relaxation kinetics even below 20 ms, as is the case of measurements with $tC^\circ/tC_{\text{nitro}}$ -labeled DNA described in Chap. 4. In this case, it is necessary to deconvolute the T-jump recovery from the observed relaxation kinetics. This deconvolution is also necessary when kinetic processes

Fig. 2.5 T-jump recovery times measured with different reference samples (*red*-fluorescence-labeled ss DNA (2008), *blue*-Cy3-labeled ss DNA (2010), and *green*-TAMRA-labeled ss DNA (2014)) at different points in time



occur on time scales that exceed ~ 20 ms, as is the case of FRET-labeled samples (TAMRA and Cy5 labels) described in Chaps 4 and 5. The deconvolution is described below.

2.2.6 Discrete Single- Or Double-Exponential Decay Convolved with T-Jump Recovery

Relaxation kinetics traces $I(t)$ measured as a function of time after the T-jump were analyzed in terms of a single-exponential decay (Eq. (2.8), with relaxation rate k_r) or double-exponential decay (Eq. (2.9), with relaxation rates k_{fast} and k_{slow}), convoluted with the recovery of the fluorescence intensity back to the pre-laser levels characteristic of the initial (equilibrium) temperature. The functional form used to fit the relaxation traces were:

$$I(t) = (I(0^+) - I_{\text{app}}(\infty)) \times \exp(-k_r t) + (I_{\text{app}}(\infty) - I(0^-)) f_{\text{rec}}(t) + I(0^-) \quad (2.8)$$

or:

$$I(t) = [I(0^+) - I_{\text{app}}(\infty)] [f_1 \exp(-k_{\text{fast}} t) + (1 - f_1) \exp(-k_{\text{slow}} t)] + [I_{\text{app}}(\infty) - I(0^-)] f_{\text{rec}}(t) + I(0^-) \quad (2.9)$$

In Eqs. (2.8) and (2.9), $I(0^+)$ and $I(0^-)$ are as defined earlier, and $I_{\text{app}}(\infty)$ is the fluorescence intensity at the end of the observed relaxation process (at $t \gg k_r^{-1}$ in Eq. (2.8) or $t \gg k_{\text{slow}}^{-1}$ in Eq. (2.9)). The parameters that were varied in a single-exponential fit are $I(0^+)$, $I_{\text{app}}(\infty)$, and k_r , and in a double-exponential fit are $I(0^+)$, $I_{\text{app}}(\infty)$, k_{fast} , k_{slow} , and f_1 , the fractional amplitude in the fast component.

2.2.7 *Acquisition and Matching of Relaxation Traces Measured Over Different Time Scales*

To acquire data with the highest temporal resolution and be able to span several decades in time, it is necessary to measure the T-jump kinetics traces over different time scales and then combine the different traces. We typically acquired the kinetics traces on at least two time scales. Most of the kinetics traces reported in Chaps 3 and 5 were obtained using the Infinium digitizer from Hewlett Packard (500 MHz, 2 GSa/s), which was eventually damaged and replaced by a new digitizer brought from Tektronix (DPO-4054B, 500 MHz, 2.5 GS/s). With the HP digitizer, typically 20,000 points were collected at each time scale such that the short time scale covered kinetics up to 2 ms, with a time-resolution of 100 ns, while the longer time scale covered kinetics up to 20 ms, with a time-resolution of 1 μ s. All the kinetic traces reported in Chap. 4 were obtained with the Tektronix digitizer, which enabled us to collect 1 M points at each time scale, thus significantly enhancing resolution and signal-to-noise in our kinetics traces. With this digitizer, the short time scale covered kinetics up to 1.6 ms, with a time-resolution of 1.6 ns, while the longer time scale covered kinetics up to 32 ms, with a time-resolution of 32 ns. The data acquired in the short time scale were reduced to 2000 points by averaging 500 points together; the data in the long time scale were reduced to 10,000 points by averaging 100 points. After averaging, the time interval between data points was 800 ns and 3.2 μ s for the short and long time scale data, respectively. Prior to any further analysis, data acquired below ~ 10 –20 μ s in each trace were discarded because of artifacts either from scattered IR laser light into the photomultiplier tube, or due to cavitation effects or from microbubbles in the samples.

In order to combine the data acquired over the two different time scales, the two traces were fitted simultaneously with a double-exponential plus T-jump recovery function (Eq. (2.9)), with an additional fitting parameter that served as a multiplicative scale factor and was applied to one of the traces to account for any systematic difference in the measured intensities for the two traces. Once appropriately scaled, the two data sets were combined into a single kinetic trace that covered the time range from ~ 10 to 20 μ s to tens of ms. These matched and combined traces were then used for all subsequent analyses. Figure 2.6a shows the kinetic trace obtained on the short time scale ($I_1(T_1)$), and the kinetic trace on the longer time scale ($I_2(T_2)$), prior to any matching. Figure 2.6b shows the kinetic traces that have been matched by scaling ($I_1(T_1)$) by a factor of 1.0065.

2.2.8 *Maximum Entropy Analysis*

Maximum entropy method (mem) is used to obtain distribution of relaxation rates. For many relaxation traces, the kinetics showed deviations from a single-exponential behavior. However, adding an additional exponential decay, while it

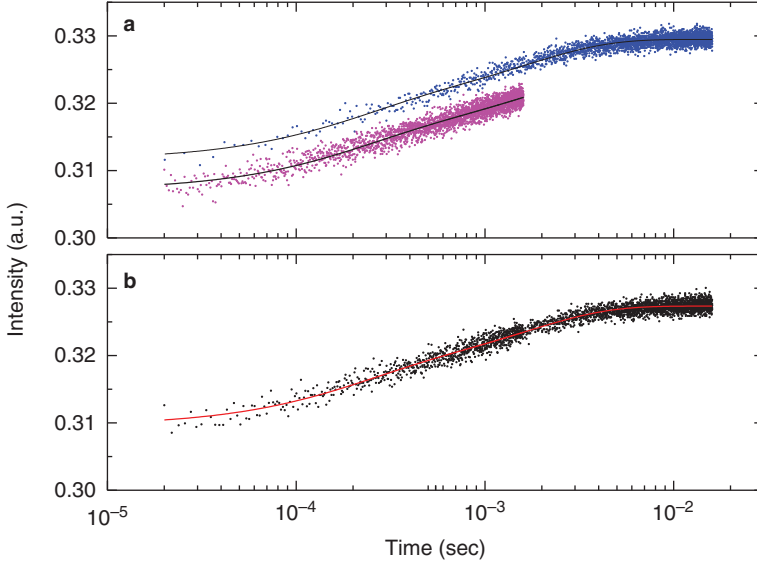


Fig. 2.6 (a) Kinetics traces taken on two separate time scales: 1.6 ms full time scale (*magenta*) and 16 ms full time scale (*blue*) and the *black* line is a two exponential fit before matching the data. (b) The combined kinetic trace obtained after scaling one data set to match the intensity of the other, as described in the text. The *red* solid line is a two exponential fit to the combined trace using Eq. (2.9)

improved the fit, gave unreliable estimates of the relaxation times and amplitudes for the two exponential components. Note that for purposes of obtaining a scale factor to match data on different time scales, a two-exponential fit was adequate. However, to overcome the limitations of such discrete exponential analysis, we chose the maximum entropy method (mem) that yields a model-independent distribution of rate constants. The mem algorithm was provided to us by Dr. Pete Steinbach of the National Institutes of Health and is described in Refs. [8–10]. The mem analysis yields a distribution $f(\log \tau)$ of relaxation times τ that maximizes the entropy S , defined below, while constraining the normalized residual sum of squares to be equal to one. The entropy function is defined as:

$$S(f, F) = \sum_{j=1}^M \left[f_j - F_j - f_j \ln \left(f_j / F_j \right) \right] \quad (2.10)$$

where f_j are the discretized values of the distribution $f(\log \tau)$ and F is a model distribution that is the default distribution in case of noisy data and is assumed to be a uniform, flat distribution.

The mem analyses on our data typically reveal two distinct peaks, which is either a combination of one relaxation phase and a slower T-jump recovery phase, or two relaxation phases, with the T-jump phase unresolved. In most cases, the two peaks

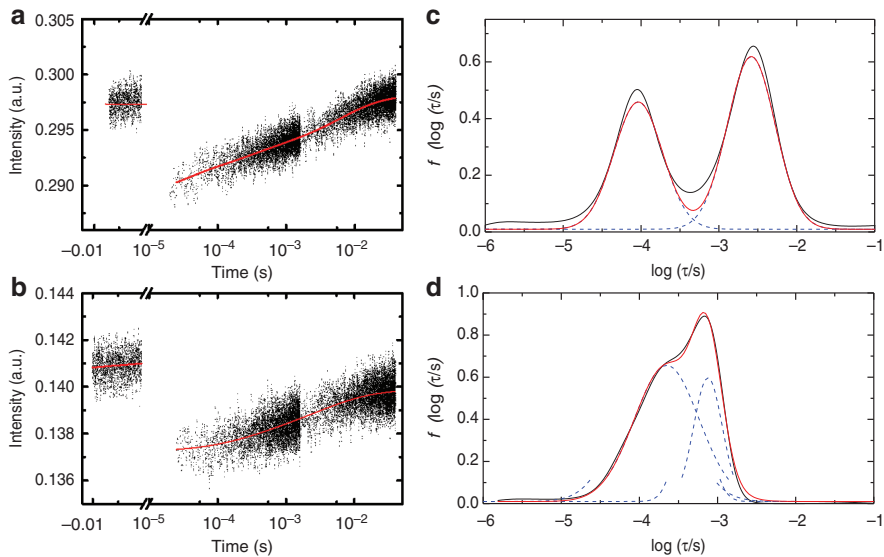


Fig. 2.7 Analysis of the distribution of relaxation times from the maximum entropy method. (a, b) Kinetics of a protein–DNA complex at two different temperatures. (c, d) The distribution of relaxation times $f(\log(\tau/s))$ is plotted versus $\log(\tau/s)$ (solid black line) in two different situations, (c) when the two peaks are not well separated (corresponding to the kinetics trace in a), (d) the second peak appears as a shoulder (corresponding to the kinetics trace in b). The two Gaussian functions that fit the distribution are shown (dashed blue line). The overall fit is also shown (red line)

were reasonably well separated, enabling us to compute an average relaxation time $\tau_{\text{ave}} = 10^{\langle \log \tau \rangle}$ for each phase, where $\langle \log \tau \rangle$ is computed from the distribution of relaxation times within each peak, and defined as:

$$\langle \log \tau \rangle = \frac{\sum_{j=1}^M \log \tau_j f(\log \tau_j) d \log \tau_j}{\sum_{j=1}^M f(\log \tau_j) d \log \tau_j} \quad (2.11)$$

If there was some overlap between the peaks, or an asymmetric peak indicating a “shoulder” suggesting two phases in the relaxation kinetics as in Fig. 2.7, the distribution $f(\log \tau)$ was fitted to the sum of two Gaussian distributions, and the average $\langle \log \tau \rangle$ was obtained from the peak position of each Gaussian distribution. The area under each Gaussian curve was used to obtain the relative amplitude in each kinetic phase.

To determine whether the observed peaks are from real relaxation phases or T-jump recovery, we also carried out mem analysis on control experiments measured on identical time scales as the relaxation kinetics, as well as on control experiments measured on a longer time scale.

2.3 Equilibrium FRET Measurements

Several methods can be used to determine the FRET efficiency on samples labeled with a donor–acceptor pair [11].

1. Measurements of lifetime of donor in the excited state, in the presence and absence of an acceptor.
2. Measurements of the donor emission intensity in the presence and absence of an acceptor.
3. Acceptor emission intensity as results of energy transfer in comparison with acceptor emission intensity from direct excitation of the acceptor.

In this study, we have used the second and third method to determine FRET efficiency values.

2.3.1 FRET Determination Using the Donor Emission

In this method, FRET efficiency in the free DNA or in complex with protein is determined by using the donor emission intensity in the presence (I_{DA}) and in the absence (I_D) of an acceptor. I_D is obtained from the donor fluorescence intensity of single-labeled (donor only) substrate, and I_{DA} is obtained from the donor fluorescence intensity of the double-labeled (donor and acceptor) substrate, under identical conditions (e.g., to find the FRET of free DNA we used donor-only free DNA and donor- and acceptor-labeled free DNA and in the case of complex it is donor-only-labeled DNA + protein and donor- and acceptor-labeled DNA + protein). The FRET efficiency value E is calculated from:

$$E = 1 - \frac{I_{DA}}{I_D} \quad (2.12)$$

2.3.2 FRET Determination from Acceptor Emission

FRET efficiency can also be measured as the increase in acceptor fluorescence intensity due to the presence of a donor fluorophore for both free and protein-bound DNA substrates. To make this measurement, the donor fluorophore was excited at donor excitation wavelength, and the emission spectra were collected covering the donor and acceptor emission. A normalized emission spectrum of a donor-only-labeled sample, excited at donor excitation wavelength, was subtracted from the emission spectrum to isolate the acceptor emission. The acceptor fluorophore was directly excited at acceptor excitation wavelength and emission spectra were

collected. The area under the corrected spectrum of acceptor emission was divided by the area under the directly excited emission spectrum to obtain the value of the acceptor ratio r_A .

$$E = \left[\frac{\varepsilon_{\lambda_A}^A}{\varepsilon_{\lambda_D}^D} \right] \left[r_A - \frac{\varepsilon_{\lambda_A}^A}{\varepsilon_{\lambda_D}^A} \right] \quad (2.13)$$

where $\varepsilon_{\lambda_D}^D$ and $\varepsilon_{\lambda_A}^A$ are the extinction coefficients at excitation wavelengths for donor and acceptor, respectively. The acceptor ratio method to determine the FRET efficiency is preferable over the donor fluorescence method because the latter requires ratio of fluorescence intensities from measurements on two separate samples, single-labeled and double-labeled DNA samples. This method for determining FRET efficiency best compensates for uncertainties in the degree of labeling of the acceptor, quantum yield of the acceptor, and the concentration of DNA used [11].

To convert acceptor ratio into real FRET efficiency requires knowledge of the extinction coefficients of the donor and acceptor fluorophores at the two different excitation wavelengths and accurate estimates of labeling efficiency. If we are only interested in variation of FRET with protein binding or variation of FRET with salt or with varying temperature, then it is not necessary to determine absolute FRET efficiency for each sample.

2.3.3 Following are the FRET Pairs Used in This Thesis

1. Conventional FRET pairs (Fluorescein and TAMRA or TAMRA and Cy5)
2. Nucleotide analogue FRET pair tC° and tC_{nitro}

1. Conventional FRET pairs (Fluorescein and TAMRA, TAMRA and Cy5)

Fluorescein (6-carboxyfluorescein (6-FAM)) (donor)/TAMRA (6-carboxytetramethylrhodamine) (acceptor) is a common donor–acceptor pair used in FRET fluorescein studies due to their good spectral overlap (Fig. 2.8a, b). Experiments reported in this thesis with 6-FAM/TAMRA FRET pair, the donor 6-FAM is excited at 488 nm which is the probe laser wavelength used in the T-jump setup and the energy is transferred to TAMRA, which then emits light centered at 580 nm. The Förster distance for this donor–acceptor pair is $R_0 = 50$ Å when the donor and/or acceptor molecules sample all possible orientations within the fluorescence lifetime of the donor, and for which $\kappa_2 = 2/3$ (see Appendix B). Another commonly used FRET pair is TAMRA/Cy5 (Fig. 2.8b, c) and in this case TAMRA's excitation wavelength was kept as 532 nm, which is the probe laser beam wavelength used in the T-jump setup to excite TAMRA. TAMRA's emission wavelength is centered at 580 nm and then due to FRET energy transfer Cy5 emits with a peak position at 662 nm. The Förster distance for

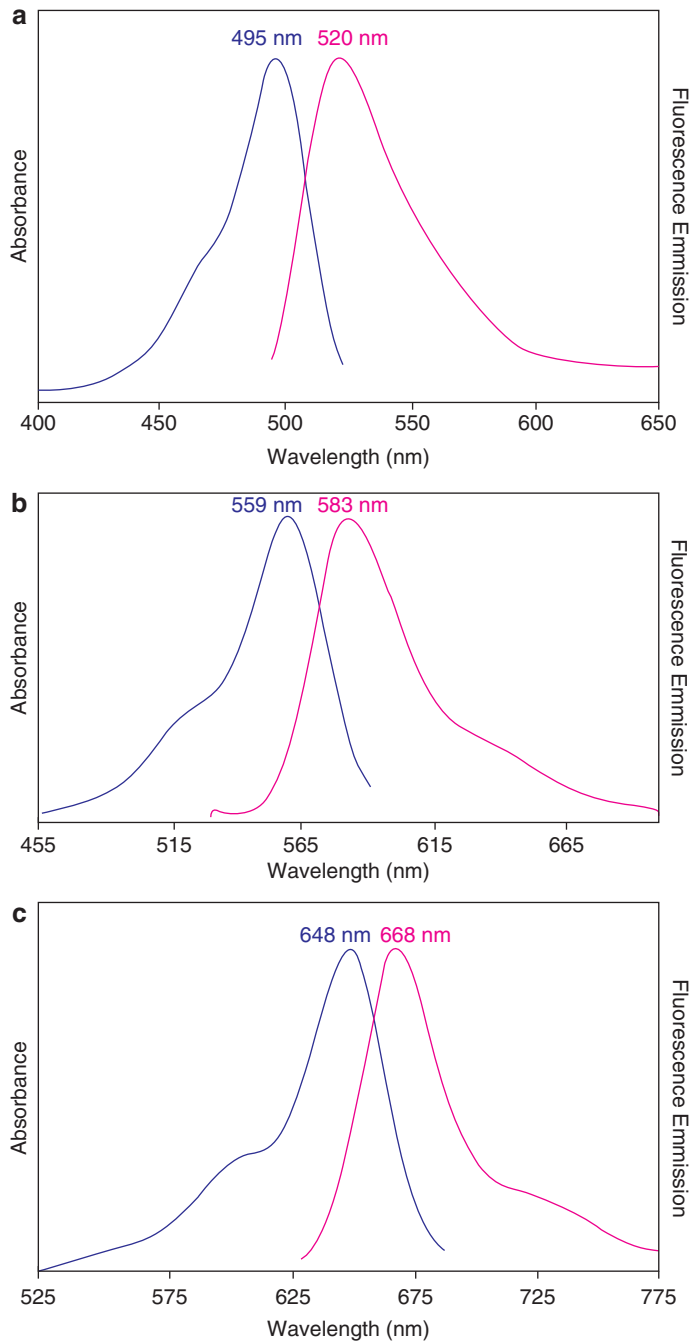


Fig. 2.8 Absorbance and emission spectra of (a) 6-FAM, (b) TAMRA, and (c) Cy5. Figures reproduced from the Integrated DNA technology (IDT) web page: <https://www.idtdna.com/site>

TAMRA and Cy5 is $R_0 = 65 \text{ \AA}$ [12]. In these FRET pairs, there are emission wavelengths where only donor emission is observed with no contribution from the acceptor. Therefore for this FRET pairs, the FRET can be measured using donor peak. For each sample, the characteristic emission intensities I_D and I_{DA} were computed as the area under the corresponding emission curves in the range $\pm 50 \text{ nm}$ around the maximum peak position. However when determining FRET using donor method, as we need two separate samples, single labeled (donor only) and double labeled (donor and acceptor), the accuracy of the concentration of the samples are crucial. The dye molecules fluorescein, TAMRA, and Cy5 are attached to oligo nucleotides via an amino C6 linker.

2. Nucleotide analogue FRET pair tC° and tC_{nitro}

The tricyclic cytosine analogue tC (1,3-diaza-2-olophnothiazine) and its oxo-homologue tC° (1,3-diaza-2-oxo-phenoxazine) was originally developed by Matteucci and coworkers in 1995 [13]. In recent years, after the elaborate characterization of these fluorescent nucleic acid bases mainly by Wilhelmsson group [14], these base analogues have emerged as novel probes with very attractive features for the study of nucleic acid structure or for investigating nucleic-acid-protein interactions. One of the striking features of these new tC products in contrast to the previously existing base analogues is that they are insensitive to their immediate surrounding bases. For example, tC is insensitive to the microenvironment in single- ($\phi_f = 0.17 - 0.24$) and double- ($\phi_f = 0.16 - 0.21$) stranded DNA and tC° is insensitive to the micro environment of double-stranded DNA ($\phi_f = 0.17 - 0.27$) (Fig. 2.9) [14]. The quantum yield of tC° in double-stranded DNA is 0.22 on average. In combination with its high molar absorptivity ($\epsilon = 9000 \text{ M}^{-1} \text{ cm}^{-1}$), tC° on average is the brightest (Brightness $\propto (\phi_f * \epsilon)$) base analogue in a duplex DNA context among the currently available base analogues [14]. However, tC° is sensitive to its surrounding bases in single-stranded DNA ($\phi_f = 0.14 - 0.41$). Though the quantum yield of tC° changes approximately by a factor of 2 between single- and double-stranded DNA, it preserves more of its high fluorescence quantum yield upon hybridization than any other base analogues [15].

Wilhelmsson et al. developed a new FRET pair consisting of tC° and another cytosine analogue tC_{nitro} (7-nitro-1, 3-diaza-2-oxophenothiazine) in order to achieve the highest possible control of donor/acceptor orientation [17]. They showed that both tC° and tC_{nitro} are rigidly stacked within the duplex and therefore are excellent candidates for FRET measurements aimed to probe the duplex conformation. Moreover, they incorporated these analogues in different sequences and with all 4 different base pairings and showed that the melting temperature of $tC^\circ/tC_{\text{nitro}}\text{---G}$ is much higher than the $tC^\circ/tC_{\text{nitro}}\text{---A,T,C}$ base pairs ($tC^\circ\text{---A,T,C}$ melting temperature is 12–26 °C lower than $tC^\circ\text{---G}$ base pair and $tC_{\text{nitro}}\text{---A,T,C}$ base-pair melting temperature is 13–19 °C lower than $tC_{\text{nitro}}\text{---G}$ base pair) [17, 18]. These results show that tC° and tC_{nitro} are highly selective for base pairing



Fig. 2.9 Fluorescence quantum yield of tC° in DNA double-stranded systems. Letters denote bases surrounding tC° (5'-...X(tC°)Y...-3'). Figure reproduced from [16]

with guanine and retain Watson–Crick pairing with guanine. In addition both tC° and tC_{nitro} slightly increase the duplex stability, melting experiments on duplex DNA with either tC° or tC_{nitro} showed that on average both of these analogues increase the melting temperature by 2 °C compared to *C*. [17]. The enhanced stability most likely comes from the increased Π – Π overlap between the extended ring system of tC° and the neighboring bases. Studies on secondary structure of tC° and tC_{nitro} incorporated duplex DNA using circular dichroism (CD) measurements showed that both tC° and tC_{nitro} sequences exhibit typical characterization of B-form DNA [16, 17]. In addition, fluorescence anisotropy measurements showed further evidence that tC° makes proper base pairing and is firmly stacked in the DNA duplex [16]. In these measurements, it was shown that the emission of tC° reports on the overall mobility of the DNA duplex without any interference from intrinsic mobility of the base analogue itself [16]. All the previous studies on tC° and tC_{nitro} confirm that incorporation of tC° or tC_{nitro} has no significant effect on the overall conformation of duplex DNA [14, 16–18].

tC° can easily be selectively excited. It has the lowest energy absorption band centered ~365 nm in duplex DNA as well as in ssDNA and the emission maximum is at 465 nm (Fig. 2.10). The lowest energy absorption maximum of the virtually non-fluorescent tC_{nitro} in dsDNA is centered at ~440 nm with an excitation coefficient of 5400 M⁻¹ cm⁻¹. This gives a very good overlap with the emission of tC° [17].

Wilhelmsson group studied the FRET efficiency of 12 different DNA sequences, in which the FRET labels were placed starting from 2 base-pair apart to 13 base-pair apart, both using steady-state measurements and time-resolved fluorescence

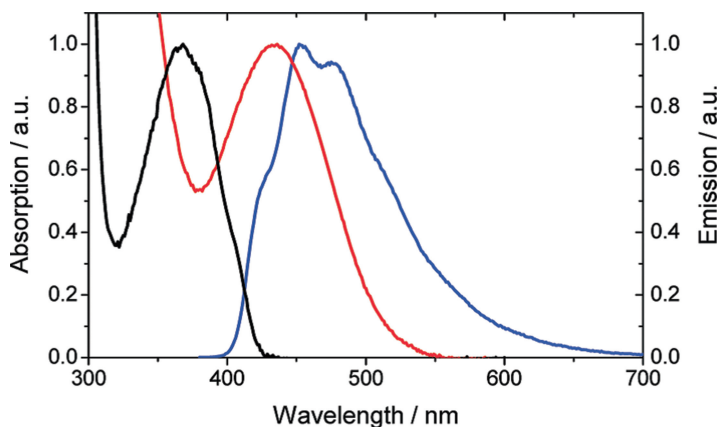


Fig. 2.10 Normalized absorption (black) and emission (blue) spectra of FRET donor tC° and absorption spectrum (red) of virtually nonfluorescent acceptor tC_{nitro} within dsDNA showing the donor/acceptor spectral overlap. Measurements performed at 22 °C in 25 mM phosphate buffer (pH 7.5) and 100 mM [Na⁺]. Figure adapted from [17] with permission. Copyright (2009) American Chemical Society

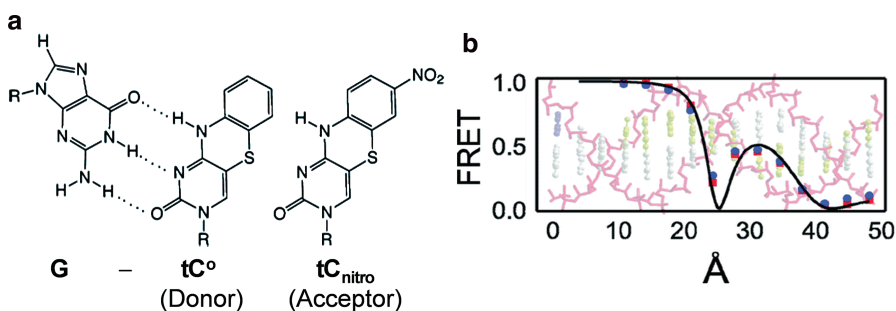


Fig. 2.11 Cytosine analogues (tC° and tC_{nitro}) act as a FRET pair and provide distance and relative orientation information in DNA. (a) Chemical structures of (left) tC° and (right) tC_{nitro} and Watson–Crick type base pairing of tC° with a guanine. (b) FRET efficiency between the tC° (donor) and tC_{nitro} (acceptor) incorporated within normal B-DNA is plotted as a function of the number of base pairs between the two probes. FRET measurements were done as described in Borjesson et al. [17]. The FRET efficiency generally decreases as the distance increases, but additionally depends on the relative orientations of the absorption and emission dipoles of the fluorophores, which changes by 2π over the helical pitch (~ 34 Å) of DNA. Figure reproduced from [17] with permission. Copyright (2009) American Chemical Society

measurements. The results showed that the efficiency is highly dependent on both distance and orientation. This is because when the distance changes the orientation of the dipole changes as well due to DNA helicity. Figure 2.11 shows the variation of FRET as a function of base-pair separation. In addition to the conventional behavior of distance dependent FRET, where FRET decreases sharply with

distance, here they observed a stepwise function which oscillates between a local maxima and minima as the orientation of the transition dipole of the donor and acceptor changes between more parallel to more perpendicular.

The $tC^\circ/tC_{\text{nitro}}$ FRET pair enables a very high control of the orientation of the donor and acceptor (hence the Förster distance) due to the fact that both the analogues are rigidly located within the base stack as well as due to a very stable donor quantum yield. If the FRET pairs are carefully chosen at the positions where the slopes are steep (Fig. 2.11) then it is possible to accurately distinguish distance from the orientation changes using FRET.

Attracted by the promising features of this newly discovered $tC^\circ/tC_{\text{nitro}}$ FRET pair, we used it to measure conformational changes in DNA upon protein binding and took advantage of a detectable change in the FRET efficiency of this pair as a consequence of a change in their separation and relative orientation upon DNA unwinding.

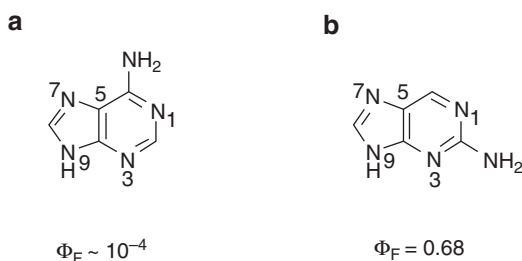
2.4 Nucleotide Analogue 2-Aminopurine (2AP)

2-Aminopurine is a fluorescence analogue of adenine nucleotide which forms hydrogen bonds with thymine very similar to those of adenine. 2AP is the most widely used fluorescent probe of DNA structure and the perturbation of that structure by interaction with enzymes and other molecules, since its potential as a fluorescence base analogue was first recognized 50 years ago. Although 2AP differs from the natural base (adenine: 6-aminopurine) only in the position of the exocyclic amine group, its fluorescence intensity is one thousand times greater [19] (Fig. 2.12).

The substitution of 2AP at a specific position of a DNA sequence preserves the structure of the double helix as 2AP hydrogen bonds and stacks with the natural bases in DNA. 2AP incorporated in DNA can be excited at 314 nm and the maximum emission occurs approximately at 370 nm. At this excitation wavelength either natural bases or the fluorescent amino acids tyrosine and tryptophan when the DNA is bound to protein will not get excited.

2AP fluoresce decreases dramatically when it is placed inside DNA (it is quenched ~ 100 times in duplex DNA compared to its free form). The main cause of this fluorescence quenching is charge transfer to the neighboring natural bases

Fig. 2.12 (a) Adenine and (b) 2AP and their fluorescence quantum yields, ϕ_F



and it is mediated by base-stacking interactions and base dynamics [20]. For this reason, 2AP is very sensitive to the protein-induced local conformations and dynamics when incorporated in DNA [21–24].

The fluorescence intensity of an extrahelical 2AP is high whereas the intensity of an intra-helical 2AP is low since 2AP is strongly fluorescent when free in solution but very weakly fluorescent when inside the DNA. Allan and Reich [21] first used this fact to monitor the methyltransferase-induced base-flipping of DNA. They showed that binding of M.EcoRI to 2AP-labeled DNA as such 2AP is placed at the target position methylation, induced a 14-fold increase in the fluorescence intensity of the 2AP. In recent years, 2AP is used to study nucleotide-flipping induced by DNA repair proteins such as MutS and Rad4 [25, 26].

2.5 Fraction of Protein and DNA in Complex at Equilibrium

Association and dissociation of protein in a simple bimolecular scheme is shown below,



The equilibrium association constant K_A can be written as:

$$K_A = \frac{f_x}{P_{eq} D_{eq}} \quad (2.15)$$

where f_x is the equilibrium concentration of the complex and P_{eq} and D_{eq} are the concentrations of free protein and DNA that are not formed as complex. Expressing P_{eq} and D_{eq} in terms of the total protein and DNA concentrations (P_o and D_o , respectively) as $P_{eq} = P_o - f_x$ and $D_{eq} = D_o - f_x$, we can write the association constant in terms of the total concentrations as:

$$K_A = \frac{f_x}{(P_o - X)(D_o - X)} \quad (2.16)$$

$$K_A[f_x - (P_o + D_o)f_x + P_o D_o] - X = 0 \quad (2.17)$$

or, in terms of the dissociation constant $K_D = \frac{1}{K_A}$, we get,

$$f_x^2 - (P_o + D_o + K_D)f_x + P_o D_o = 0 \quad (2.18)$$

Thus, for a given value of P_o , D_o and K_D , we obtain the concentration in complex as:

$$f_x = (P_o + D_o + K_D) \pm \frac{\sqrt{(P_o + D_o + K_D)^2 - 4P_o D_o}}{2} \quad (2.19)$$

Only the solution with minus sign in Eq. (2.19) gives physically meaningful values for f_X , which cannot be larger than D_o

$$f_X = (P_o + D_o + K_D) - \frac{\sqrt{(P_o + D_o + K_D)^2 - 4P_o D_o}}{2} \quad (2.20)$$

2.6 K_D Measurements from Equilibrium FRET

2.6.1 *Conventional Titration Experiments*

Assuming only two states for the protein and DNA, free and in complex, the measured FRET efficiency E or acceptor ratio r_A depend on the fraction of DNA in complex f_X as follows:

$$\begin{aligned} E &= E_X f_X - E_{\text{free}}(1 - f_X) \\ r_A &= r_A^X f_X - r_A^{\text{free}}(1 - f_X) \end{aligned} \quad (2.21)$$

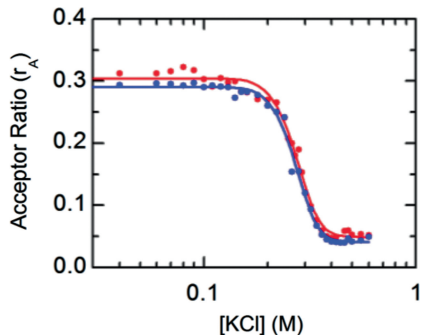
where E_X (r_A^X) is the FRET efficiency (acceptor ratio) for the complex, E_{free} (r_A^{free}) is the FRET efficiency (acceptor ratio) for free DNA substrate, and f_X is obtained from Eq. (2.20) with the condition $P_o \geq D_o$.

K_D of protein–DNA complexes can be determined from equilibrium titration measurements. Typically, the FRET versus [protein] was measured in about 15–20 samples containing a fixed concentration of DNA (~1–10 nM) and varying concentrations of protein. These binding isotherms were obtained for [KCl] ranging from 100 to 500 mM, and the corresponding K_D values were obtained from nonlinear least-squares fit to the data using Eqs. (2.20) and (2.21) with K_D and E_X as free parameters and with E_{free} is determined with free DNA sample. However, this method is inaccurate in determining K_D values smaller than about 2 nM as we need to keep the fixed DNA concentration during titration less than the K_D value of the complex we are aiming to determine and since the signal from DNA concentrations below 2 nM is comparable to the background noise (instrument limitation), a high level of fluctuations observed in the measured signal.

2.6.2 *Salt Titration Experiments [27]*

To obtain reliable K_D values in the sub-nanomolar range from equilibrium measurements, we have used an alternative approach in which we exploit the expected linear dependence of $\log(K_D)$ versus $\log([KCl])$. We measured the acceptor ratio in

Fig. 2.13 Binding affinity measurements on mutant IHF (α R21C)-H' complex by salt titration-binding isotherms. The acceptor ratio of the complexes is plotted as a function of [KCl] at 25 °C



about 20–25 samples containing a fixed protein–DNA concentration, but with [KCl] ranging from ~ 10 to ~ 700 mM. Increasing the salt concentration destabilizes the complex, thus decreasing the fraction of DNA in complex, and the acceptor ratio drops from a value characteristic of complex at low [KCl] ($f_X \approx 1$) to a value characteristic of the fraction in complex at high [KCl] ($f_X \approx 0$). To simulate f_X versus [KCl], we use Eq. (2.20), and parameterize the salt dependence of K_d as follows:

$$K_D = K_{D_0} \left(\frac{[\text{KCl}]}{[\text{KCl}]_0} \right)^{SK_d} \quad (2.22)$$

where K_{D_0} is the dissociation constant at a reference salt concentration $[\text{KCl}]_0$ and SK_d is the expected slope on a $\log(K_D)$ versus $\log([\text{KCl}])$ plot. The measured acceptor ratio versus [KCl] data is then described in terms of Eqs. (2.20), (2.21), and (2.22), with four free parameters: K_{D_0} , SK_d , r_A^X , and r_A^{free} , and the best fit parameters that minimize the residuals are obtained from a Monte Carlo search in parameter space [28]. For a fixed value of the reference $[\text{KCl}]_0$, we carried out 20 independent Monte Carlo searches in parameter space for each set of measurements to ensure a global minimum in the residual chi-squares. A typical plot of salt dependence titration is shown in Fig. 2.13. The K_D values at different [KCl], and the slope parameter SK_d , reported in Table 3.4 in Chap. 3, are the mean values obtained from the best fits of two independent sets of measurements and the errors are the statistical variations obtained from the separate fits. The dominant source of error in determining K_D at a given salt concentration comes from the uncertainty in the determination of the slope SK_D . The results of Table 3.4 are independent of our choice of the reference $[\text{KCl}]_0$, which was varied between 100 and 300 mM KCl, to check for consistency.

References

1. C.F. Bernasconi, *Relaxation Kinetics* (Academic, New York, 1976)
2. H. Staerk, G. Czerlinski, Nanosecond heating of aqueous systems by giant laser pulses. *Nature* **205**, 63–64 (1965)
3. R. Rigler, A. Jost, L. De Maeyer, Chemical kinetics at micro level—a laser micro temperature jump apparatus for relaxation studies in micro samples. *Exp. Cell Res.* **62**, 197–203 (1970)
4. C.M. Phillips, Y. Mizutani, R.M. Hochstrasser, Ultrafast thermally-induced unfolding of RNase-A. *Proc. Natl. Acad. Sci. U. S. A.* **92**(16), 7292–7296 (1995)
5. J. Kubelka, Time-resolved methods in biophysics. 9. Laser temperature-jump methods for investigating biomolecular dynamics. *Photochem. Photobiol. Sci.* **8**(4), 499–512 (2009)
6. P.A. Thompson, W.A. Eaton, J. Hofrichter, Laser temperature jump study of the helix-coil kinetics of an alanine peptide interpreted with a ‘kinetic zipper’ model. *Biochemistry* **36**(30), 9200–9210 (1997)
7. W.O. Wray, T. Aida, R.B. Dyer, Photoacoustic cavitation and heat transfer effects in the laser-induced temperature jump in water. *Appl. Phys. B* **74**, 57–66 (2002)
8. A.K. Livesey, J.C. Brochon, Analyzing the Distribution of Decay Constants in Pulse-Fluorimetry Using the Maximum Entropy Method. *Biophys. J.* **52**(5), 693–706 (1987)
9. P.J. Steinbach, R. Ionescu, C.R. Matthews, Analysis of kinetics using a hybrid maximum-entropy/nonlinear-least-squares method: application to protein folding. *Biophys. J.* **82**, 2244–2255 (2002)
10. P.J. Steinbach, Inferring lifetime distributions from kinetics by maximizing entropy using a bootstrapped model. *J. Chem. Inf. Comput. Sci.* **42**(6), 1476–1478 (2002)
11. R.M. Clegg, Fluorescence resonance energy transfer and nucleic acids. *Methods Enzymol.* **211**, 353–388 (1992)
12. L.E. Sass et al., Single-molecule FRET TACKLE reveals highly dynamic mismatched DNA-MutS complexes. *Biochemistry* **49**(14), 3174–3190 (2010)
13. K.-Y. Lin, R.J. Jones, M. Matteucci, Tricyclic-2'-deoxycytidine analogs:synthesis and incorporation into oligodeoxynucleotides which have enhanced binding to complementary RNA. *J. Am. Chem. Soc.* **117**, 3873–3874 (1995)
14. L.M. Wilhelmsson, Fluorescent nucleic acid base analogues. *Q. Rev. Biophys.* **43**, 159–183 (2010)
15. P. Sandin et al., Fluorescent properties of DNA base analogue tC upon incorporation into DNA—negligible influence of neighbouring bases on fluorescence quantum yield. *Nucleic Acids Res.* **33**(16), 5019–5025 (2005)
16. P. Sandin et al., Characterization and use of an unprecedentedly bright and structurally non-perturbing fluorescent DNA base analogue. *Nucleic Acids Res.* **36**(1), 157–167 (2008)
17. K. Borjesson et al., Nucleic acid base analog FRET-pair facilitating detailed structural measurements in nucleic acid containing systems. *J. Am. Chem. Soc.* **131**(12), 4288–4293 (2009)
18. K. Borjesson, P. Sandin, L.M. Wilhelmsson, Nucleic acid structure and sequence probing using fluorescent base analogue tC°. *Biophys. Chem.* **139**, 24–28 (2009)
19. A. Jones, R.K. Neely, 2-aminopurine as a fluorescent probe on DNA conformation and the DNA-enzyme interface. *Q. Rev. Biophys.* **48**, 244–279 (2015)
20. E. Rachofsky, R. Osman, J.B. Ross, Probing structure and dynamics of DNA with 2-aminopurine: effects of local environment on fluorescence. *Biochemistry* **40**, 946–956 (2001)
21. N.O. Reich, B.W. Allan, Targeted base stacking disruption by the EcoRI DNA methyltransferase. *Biochemistry* **35**, 14757–14762 (1996)
22. M.W. Frey, L.C. Sowers, D.P. Millar, S.J. Benkovic, The nucleotide analog 2-aminopurine as a spectroscopic probe of nucleotide incorporation by the Klenow fragment of Escherichia coli polymerase I and bacteriophage T4 DNA polymerase. *Biochemistry* **34**, 9185–9192 (1995)
23. D.J. Krosky, F.H. Song, J.T. Stivers, The origins of high-affinity enzyme binding to an extrahelical DNA base. *Biochemistry* **44**, 5949–5959 (2005)

24. R.K. Neely, D. Daujotyte, S. Grazuili, S.W. Magennis, D.T. Dryden, S. Klimasauskas, A.C. Jones, Time-resolved fluorescence of 2-aminopurine as a probe of base flipping in M. HhaI-DNA complexes. *Nucleic Acids Res.* **33**, 6953–6960 (2005)
25. E. Jacobs-Palmer, M.M. Hingorani, The effects of nucleotides on MutS-DNA binding kinetics clarify the role of MutS ATPase activity in mismatch repair. *J. Mol. Biol.* **366**(4), 1087–1098 (2007)
26. X. Chen et al., Kinetic gating mechanism of DNA damage recognition by Rad4/XPC. *Nat. Commun.* **6**, 5849 (2015)
27. P. Vivas et al., Mapping the transition state for DNA bending by IHF. *J. Mol. Biol.* **418**(5), 300–315 (2012)
28. S.V. Kuznetsov et al., Loop dependence of the stability and dynamics of nucleic acid hairpins. *Nucleic Acids Res.* **36**, 1098–1112 (2008)

Dynamics and Mechanism of DNA-Bending Proteins in
Binding Site Recognition

Velmurugu, Y.

2017, XXI, 199 p. 112 illus., 105 illus. in color.,

Hardcover

ISBN: 978-3-319-45128-2